Research Square

Preprints are preliminary reports that have not undergone peer review.
They should not be considered conclusive, used to inform clinical practice,
or referenced by the media as validated information.

Highly Efficient Heterojunction Nanocatalyst Fe 0 - Ag 0 @BN in the Degradation of Alizarin Yellow (AY): A greener and sustainable approach

Youna Jo
Kangwon National University
Diwakar Tiwari
Mizoram University
Daeik Kim
hg2wjms@gmail.com

EST & ES, Inc
Yongbum Choi
Kangwon National University
Yiyong Yoon
Catholic Kwandong University
Taylor MJ Kim
EST & ES, Inc
Joonseok Park
Kangwon National University

Research Article

Keywords: Green synthesis, Bimetallic nanocatalyst, Photo-Fenton-like process, Alizarin Yellow, Nanoscale Zero-valent Iron (nZVI), LED-visible light treatment

Posted Date: March 27th, 2026

DOI: https://doi.org/10.21203/rs.3.rs-8126662/v1

License: This work is licensed under a Creative Commons Attribution 4.0 International License.
Read Full License

Additional Declarations: No competing interests reported.

Highly Efficient Heterojunction Nanocatalyst Fe^0-Ag^0@BN in the Degradation of Alizarin Yellow (AY): A greener and sustainable approach

Youna Jo[1], Diwakar Tiwari[2], Daeik Kim[3,*], Yongbum Choi[1], Yiyong Yoon[4], Taylor MJ Kim[3], and Joonseok Park[1]

[1]Department of Earth and Environmental Engineering, Kangwon National University, Samcheok, Gangwon-do 25913, South Korea

[2]Department of Chemistry, School of Physical Sciences, Mizoram University, Aizawl-796004, India

[3]EST & ES, Inc., Fullerton, CA 92833, USA

[4] Department of Environmental Engineering, Catholic Kwandong University, Gangneung, Gangwon-do 25601, South Korea

*Author for correspondence: Phone: 1-213-820-3156, Email: Hg2wjms@gmail.com

ABSTRACT

The textile, paper, and chemical industries, including dye or pigment create significant quantities of wastewater streams that are typically released into surface water resources, thus contaminating aquatic environment. Among them, several dye chemical compounds are highly hazardous, even though in some concentration, resulting in endangering the flora and fauna of the aquatic environment. This study seeks to remove a dye pollutant, Alizarin Yellow (AY), from polluted aqueous solutions using novel bimetallic Fe & Ag nanoparticles supported with bentonite (Fe^0-Ag^0@BN). Various analytical techniques extensively characterize nanocomposite materials and show a distinct distribution of Ag and Fe nanoparticles onto the nanocomposite. The nanocomposite is highly efficient in removing the Alizarin Yellow in the Fenton-like process. The nanocatalyst in batch reactor eliminated AY (2 mg/L) in 30 and 60 min, using UV-A and LED irradiation, respectively. Under the UV-A irradiation, the process mineralizes a high percentage of AY (98%). Furthermore, the presence of silver nanoparticles synergized the degradation process, and an enhancement of Fe(II) in the bulk solution positively impacted the elimination of AY in the light-illuminated Fenton-like process, as well. The nanocatalyst (nanoscale Zero-valent Iron: nZVI) exhibited a reasonable stability and

reusability in the batch processes, and excellent selectivity in AY elimination using different natural water samples. The bimetallic Fe^0-Ag^0@BN nanocatalyst composite showed the potential for the removal and mineralization of AY in aquatic environment.

Keywords: Green synthesis · Bimetallic nanocatalyst · Photo-Fenton-like process · Alizarin Yellow · Nanoscale Zero-valent Iron (nZVI) · LED-visible light treatment

1. Introduction

Hazardous compounds often found in industrial wastewater prompted the development of innovative solutions to protect aquatic or marine life from these pollutants. The textile industries are the primary contamination source because of the unregulated qualitative and quantitative release of industrial effluents into the aquatic environment, which leads to serious public health and ecological concerns, and a severe environmental hazard (Lalliansanga et al. 2022). The ratio of BOD to COD of the typical textile industry wastewater stream is approximately 0.25, indicating that the wastewater includes a significant quantity of non-biodegradable organic content. The dyeing and finishing (D&F) industries detrimentally contribute such organic matter to the waterbodies (Liang et al. 2012). The broad range of dyes that often contribute to the pollution of water bodies is equivalently prevalent in the leather, cosmetic, food, plating, photo-electrochemical cells, wood, and pulp & paper industries (Adlnasab et al., 2017).

The most significant and widely used dyes include azo, anthraquinone, indigo-ide, phthalocyanine, triarylamine ethane, triphenyl methane, sulphur, etc. (dos Santos et al., 2007). Alizarin Yellow (AY), 5-[(p-Nitrophenyl) azo] salicylic acid sodium salt, is an azo-dye pigment group synthesized by the diazo coupling method, which is commonly utilized in the paint and lacquer, textile, leather, plastic, culinary, and pharmaceutical sectors (Lalliansanga et al., 2020). The textile industry uses Alizarin Yellow (AY) as a pigment. AY's aromatic rings have a complex structure that makes them resistant to biodegradation, leading to harmful effects on the lungs and mucosal membranes of human organs. So, AY becomes dangerous once absorbed by the skin, breathed, or ingested with severe health impacts on the eyes, skin, and respiratory system (Ogugbue and Sawidis, 2011; Przystaś et al., 2012). The physical-chemical methods, such as adsorption, advanced oxidation, anaerobic and aerobic biological processes, coagulation-flocculation, electrochemical, and various hybrid treatment

technologies, treat the wastewater containing various azo dye compounds (Liang et al. 2012). However, such methods possess several inherent limitations, including high operational cost, large sludge production, the efficiency of the method, by-products formed (sometimes more toxic than the dye itself), and relatively low effectiveness of cost versus investment and requirement of advanced and more efficient treatment in the following step. The textile industry should cope with economic and ecological challenges, expanding the possibility of reusing massive wastewater and plant effluents. Therefore, research and development (R&D) of more efficient, affordable, and sustainable water treatment technologies for dye degradation becomes necessary.

Advanced oxidation processes (AOPs), which primarily rely on the *in-situ* creation of highly reactive hydroxyl radicals (•OH) with an oxidation potential (E^0) of 2.80V vs. SHE seem to be an intriguing alternative to several conventional methods for the mineralization of pollutants (Pera-Titus et al., 2004; Kim et al., 2010) and the degradation of recalcitrant organic contaminants (Kumar and Dutta, 2022). The heterogeneous photo-Fenton-like operations have been considered viable and efficient AOPs for preventing secondary pollution while degrading and mineralizing the organic contaminants in wastewater (Zhang et al., 2019; Kim et al., 2010). Depending on their electronic structures, the materials are utilized as catalysts in the light-assisted redox reactions. The filled valence and unoccupied conduction bands characterize the electronic structure. The easiness with which a catalyst produces an electron-hole pair determines its reactivity. Free radicals are created when these electron-hole pairs interact with the substrate (Tahir et al., 2020).

The development of nanotechnology and the rapid advancement of nanomaterials advanced the research owning to a good number of nanomaterials' superior structural, morphological, electronic, optical, and mechanical properties. These materials possess a high surface-to-volume ratio, unique electrochemical properties, high chemical reactivity, increased activity, and relatively high optical properties (Rodney et al., 2018). Nanoscale zero-valent iron (nZVI) is one of the most effective materials for organic pollution clean-up, successfully being integrated in Fenton-like reactions (Kecić et al. 2018). The nZVI/H_2O_2-Fenton method is very useful to removing highly recalcitrant contaminants, including pharmaceuticals, chlorinated organics, nitroaromatics, and organic dyes (Lin and Hsu, 2018). nZVI slowly releases the soluble Fe^{2+}, which is necessary for the H_2O_2 activation to form •OH radicals. Bimetallic nanocomposites derived from the nZVI and some other metals (M/nZVI) have been found to enhance the sensitivity of nZVI nanoparticles and reduce oxidation on the catalyst's outer surface (Ulucan-Altuntas and Kuzu, 2019; Yamaguchi et al., 2018). In a line, the silver

nanoparticles (Ag(NPs)) are effective in treating wastewater from different source streams such as industrial, sewage, textile, personal care, paint, and food supplements (He et al., 2014; Marimuthu et al., 2020). One of the significant disadvantages of nanoparticle product was a tendency of becoming agglomerated. However, a suitable support medium was found to prevent the agglomeration of nanoparticles that are interlayer clays (Herney-Ramirez et al., 2010), biochar (Wang et al., 2021), activated carbon (Ramirez et al., 2007), ashes (Flores et al., 2008), and polymeric resins (Liou et al., 2005). The support medium increases the real applicability of the material in photo-Fenton processes, resulting in improving stability and reactivity of nanocatalysts. Indigenous clay is a promising support medium because of its natural abundance, large surface area, non-toxic, low cost, and relatively fair stability (Herney-Ramirez et al., 2010). Bentonite is widely used to treat various industrial wastes (Banat et al., 2000) and, perhaps, is promising as a support medium for designing newer advanced materials. Therefore, the present work aims to synthesize the bimetallic nanocatalyst employing bentonite clay as a support medium. The Fe and Ag nanoparticles are dispersed with such support, and the "Greener Approach" synthesizes these nanoparticles *in situ*. The material was employed in the proficient Alizarin Yellow (AY) removal from an aqueous stream, using different light sources in the photo-Fenton-like reactions. The kinetic study of degradation and reusability of the catalyst with analytical results envisages the high potential of usage in various unit operations of treatment sectors

2. Materials and Methods

2.1 Experimental procedures

2.2.1 Leaf extract and solid nanocomposite preparation

The guava leaves were prepared from the guava trees inside the institute's campus (Mizoram Central University, India), which are thoroughly washed with water and rinsed with DI water before being dried for 3 h at 90 °C. A grinder was used to grind up the dried leaves to obtain a fine powder of leaves. In a 250 mL conical flask, 10 g of powdered leaves were mixed with DI water (100 mL). After heating at 80 °C for 20 min, filtered in Whatman No. 1 filter paper and the extracted liquid was kept at 4°C for the later use of experiments.

The prepared guava extract took part in the *in-situ* generation of the Fe^0 and Ag^0 nanoparticles. The precursors' proportion ratio in the nanoparticle synthesis was also optimized. An accessible technique produced the (Fe^0@BN) and Fe^0-Ag^0@BN catalysts (nFLC). Bentonite powder (15 g) was suspended with $FeNO_3$ solutions (250 mL of 0.1 mol/L) for 8 h at room temperature, while slowly being stirred. Centrifugation at 1,500 rpm separated the suspension and the solid from the emulsion

Further to the Fe^{2+}@BN suspension, 75 mL of guava leaf extract was added with 15 g of solid, and 10 h of stirring of the suspension resulted in the Fe^0-Ag0@BN nanocomposite. Similarly, the Fe^{2+}-Ag^+@BN suspension was obtained by taking the precursors in 250 mL of 2.5 mmol/L $AgNO_3$ solutions and being stirred for 6 h. The Fe^{2+}-Ag^+@BN suspension was transferred to a flask, and then 75 mL of guava leaf extract was gradually added and stirred for 6 h. The small solid particles present were separated from the liquid by centrifugation and several consecutive washings removed the extra NO_3^- ions. Such solid particles were in a hot air oven at 50 °C for 5 h. The grinding of nanocomposite materials resulted in a fine powder of solid materials and was placed in an airtight polypropylene container.

2.2.2 *Photo-catalysis procedure and quantification techniques*

A constant quantity (50 mg/L) of AY was dissolved in purified water to create a standard stock solution. The desired experimental concentrations were obtained by diluting the stock solution. The catalysts, pristine bentonite (BN), Fe0@BN, or Fe0-Ag0@BN were used in the batch experiments to investigate the degradation of AY. UV-A (Philips, 9W, Netherland) and LED (Havells, 9W, India) lamps assisted in the photo-Fenton-like processes. The kinetic study on the degradation of the target contaminant was carried out using the time-dependence degradation under the photo-Fenton-like operations employing nanocomposite catalyst Fe0-Ag0@BN. The parameters viz., pH, Fe0-Ag0@BN dose, and H2O2 dosage, were chosen to optimize the degradation efficiency. In addition, the effect of pollutants' concentration and interfering ions was extensively studied in the degradation process. The photo-Fenton-like degradation efficiency and non-purgeable organic carbon removal were obtained in the degradation of the target pollutant at varied concentrations. In addition, the reusability of the Fe0-Ag0@BN nanocatalyst in the degradation of AY was examined in repeated cycles of operation. For the reusability study, the used nanocomposite materials were separated by centrifugation after each treatment step, rinsed with distilled water, dried (80 °C in a hot air oven), and crushed using a mortar pestle, and the catalyst powder was used in subsequent runs.

The experiments were carried out in a self-built water bath, and the temperature was maintained at 25 ± 1°C. The degradation experiments were carried out in a 100 mL borosilicate reactor placed onto a magnetic stirrer plate and maintained at a constant stirring speed (300 rpm). The reactor is appropriately covered with parafilm and placed inside a self-made dark cabinet. A known amount of nanocatalyst powder was dispersed in pollutant solutions, and the suspension was stirred in the dark for 60 min to reach adsorption/desorption equilibrium. Just after the equilibrium time, the optimized amount of H2O2 concentration was injected. The photo-Fenton-like process was initiated immediately after the addition of H2O2 by irradiating the solution mixture either by a UV-A or a LED source. The quantitative estimation of AY was performed by UV-VIS spectrophotometer (Shimadzu, Japan, model: UV-1800), using an HPLC system (High-Performance Liquid Chromatography, Waters, Model: Waters 515 HPLC pump; USA) fitted with a UV detector (Waters, Model: Waters 2489 UV/VIS Detector; USA). Cross-checks were performed. Various time intervals (e.g., 10, 20, 30, 45, 60, 90, 120 min) were used to collect the supernatant of the treated pollutant samples for measurement. Before being tested with a UV-Vis Spectrophotometer or an HPLC to ascertain unknown quantities, the supernatant solution was filtered using a syringe filter (0.25 µm; Whatman, USA). Unknown pollutant concentrations were assessed using a C18 analytical column (4.6 x 250 mm, pore size 100.0 Å) with mobile phases of water (HPLC grade, Himedia), and acetonitrile (HPLC grade, Himedia) at a 70:30 ratio, at 0.5 mL/min and a 20 min run time. The pollutant, AY has λmax of 353 nm. As a result, the calibration line was obtained at its corresponding wavelength using the standard pollutant solutions. To check for deviations and errors in the results, every experiment was run three times.

3. Results and Discussion

3.1 Phytochemical Screening

The qualitative screening, using a known method described elsewhere, demonstrates the presence of several phytochemicals in the leaf extract (Chandraker et al., 2020) and is displayed in Table 1. The presence of flavonoid and alkaloid phytochemicals derives the Ag^{+}/Fe^{3+} ions

to their zero-valent state and stabilizes the nanoparticles in the solid matrix of the integrated composite.

3.2 Characterization of the Integrated Composite

3.2.1 pH_{PZC}, Band-gap Energy, and BET Surface Area Analyses

A standard acid-base titration method determined the point of zero charges (pH_{PZC}) of bentonite (BN), Fe^0@BN, and Fe^0-Ag^0@BN nanocatalysts and was found to be 7.2, 6.3, and 6.7, respectively. The diffuse reflectance spectroscopy (DRS) results were utilized to draw the Tauc graphs ($h\upsilon$ *vs.* $(\alpha h\upsilon)^2$) and hence, calculated the band gap (E_g) energies of these solids, i.e., BN, Fe^0@BN, and Fe^0-Ag^0@BN (*Cf* figure S1(a)) (Lalliansanga et al., 2022). The E_g values were 3.25 eV for bentonite, 2.23 eV for Fe^0@BN, and 2.15 eV for Fe^0-Ag^0@BN. The significantly low values of E_g seemed to successfully activate the nanocomposite with the visible-light sources and achieved the required efficiency of the catalyst (Djellabi et al., 2022).

Figure 1 depicts the materials' N_2 adsorption/desorption isotherms. These solids possess Type IV isotherms with H3 hysteresis loops, demonstrating the solid's mesoporous structure (Bounab et al., 2017). Fe^0@BN and Fe^0-Ag^0@BN pore diameters were 91.0861 and 0.0993 cm3/g, respectively. The specific surface areas of 62.59, 36.48, and 8.59 m2/g were obtained for the bentonite, Fe^0@BN, and Fe^0-Ag^0@BN solids, respectively. Because of the pores and the predominantly dispersed nanoparticles on the bentonite clay surface, the addition of Fe(NPs) and Ag(NPs) significantly reduced the specific surface area of the solids. In addition, Figure 2 displays that the distribution of pore sizes for these solids and the desorption peak at the pore width of 40 Å was found for the bentonite, whereas the solids of Fe^0@BN and Fe^0-Ag^0@BN displayed a peak of around 15 Å in the adsorption pore distribution data.

3.2.2 Morphological Study of Nanocomposite Solids

The Scanning Electron Microscopy (SEM) and the Transmission Electron Microscopy (TEM) images were employed to estimate the particle size of the newly designed nanocomposite solids of Fe^0@BN, Fe^0-Ag^0@BN and to assess the morphological analyses. The SEM depictions of the BN, Fe^0@BN, and Fe^0-Ag^0@BN examined the surface structure of the materials (Fig. 1). The SEM image found that the bentonite possesses a heterogenous and layered structure in Fig.

1(a). However, the Fe or Ag nanoparticles occupied the surface of bentonite in the composite materials, i.e., Fe^0@BN and Fe^0-Ag^0@BN in Fig. 1(b) and 1(c), thus enhancing the surface heterogeneity of solids. These solids contain C, O, Na, K, Al, Ti, Fe, Si, and other elements, according to the Energy Dispersive X-ray (EDX) spectra in Fig. 1 (d), (e), and (f). However, the nanocomposite solid Fe^0-Ag^0@BN clearly showed the presence of an Ag peak, signifying the occurrence of silver (Ag) in the solid in Fig. 1(f). Furthermore, as shown in Fig. 1 (g) and 1 (h) of the Fe^0@BN and Fe^0-Ag^0@BN materials' TEM images, the nanocomposite of Fe^0@BN solid showed the dispersion of Fe(NPs) over the bentonite's surface, and the approximate size of the particles was *Ca.* 14.0 nm. The iron (Fe(NPs)) nanoparticles were evenly distributed over the surface and did not aggregate. The d-spacing of the fringes on the iron nanoparticles was 0.17 nm (Fig. 1(g)). Similarly, the Ag nanoparticles were evenly scattered all over the surface layer of the bentonite in the nanocomposite Fe^0-Ag^0@BN solid in Fig. 1(h). The average particle size in the Ag(NPs) (220) plane was 12.0 nm, and the silver nanoparticles on the clay surface were spherical and were not clumped together.

3.2.3 XRD and XPS Spectroscopic Analysis

Figure 2(d) displays the results of X-Ray diffraction (XRD) spectra of the bentonite, Fe^0@BN, and Fe^0-Ag^0@BN solids. The bentonite contained the kaolinite, illite, quartz, and smectite phases since distinct diffraction peaks were observed in the XRD diffraction pattern of such solids (Dihingia and Tiwari, 2022). Diffraction at the 2θ value of 45° confirmed the presence of Fe(NPs) in the Fe^0@BN and Fe^0-Ag^0@BN solids (Fig. 2(d)) (Sulaiman and Al-Jabari, 2021). Further, the Fe^0-Ag^0@BN solid's XRD peaks inferred the characteristic diffraction peaks of Ag(NPs) (JCPDS file No. 01-087-0719).

In addition, the X-ray photoelectron spectroscopic (XPS) graph of the Fe^0-Ag^0@BN indicated that iron (Fe), silver (Ag), and oxygen (O) were presented in the survey scan (Fig. 3), where the 2p and 3d peaks of Fe and Ag were displayed, respectively. The XPS peak confirmed the presence of Fe(0) in the nanocomposites at 706.4 eV (Ye et al., 2021). Similarly, the $3d_{5/2}$ and $3d_{3/2}$ at the binding energies of 368.5 and 374.2 eV, respectively, validated the presence of Ag^0 (Prieto et al., 2012). Thus, in the Fe^0-Ag^0@BN nanocomposite solid, both iron and silver were present in their zero valent oxidation states.

3.3 Photo-assisted Fenton-like Degradation of AY

3.3.1 pH Dependence Degradation

In the Fenton or Fenton-like process, the initial pH plays a crucial role in regulating the production of hydroxyl radicals (•OH) and the breaking down of zero-valent (Fe(NPs)), which in turn dictates the degradation efficiency (Midik Ertosun et al., 2019). The most optimum pH of operation was obtained from several tests at the pH range of 2 and 7. The batch reactor performed the experiments using a catalyst dosage of 100 mg/L, H_2O_2 (0.1 mL/L), and an AY concentration of 2 mg/L. In Fig. 4, the degradation percentages of AY as a function of pH was exhibited, and a relatively lower pH range of 2 to 4 favoured the removal of AY, using the Fe^0-Ag^0@BN nanocatalyst. At the pH of 3, the AY degradation efficiency of *Ca.* 93.54 % was achieved, whereas a further increase in pH (e.g., pH > 3.0) significantly decreased the efficiency of the AY degradation. In other words, the AY degradation efficiency, from 64 to 14 %, was caused by increasing pH from 5.0 to 7.0. The results inferred that the acidic environment was favorable for the AY degradation since its lower pH boosted the Fe(NPs) corrosion and excess formation of •OH radicals. The equations (1) and (2) demonstrate the reaction mechanisms.

$$Fe(III)\ H_2O_2 \rightarrow Fe(II) + H^+ + HOO\bullet \quad (1)$$

$$HO\bullet + H^+ + e^- \rightarrow H_2O \quad (2)$$

The explanation for the reduction in AY degradation efficiency by the nanocatalyst under certain pH circumstances was the suppression of Fe(II) release to the bulk of the pollutant solution, which ended up hindering the generation of hydroxyl radicals (OH•), as specified in Equation (1) (Guo et al., 2019). Additionally, the oxidation potential of OH• radical became reduced in the alkaline solutions, reducing the degradation efficiency (Fida et al., 2017a). The instability of H_2O_2 causes it to disintegrate into smaller molecules like molecular oxygen (O_2) without generating a substantial amount of OH•. As a result, the degradation percentage at pH > 3.0 rapidly fell off. At optimum experimental conditions, the $\bullet O_2$ feebly decomposed organic contaminants (Zhan et al., 2022). With increasing solution pH, the Fenton reagent's activity decreased. This effect is attributable to less reactive trivalent iron hydroxide formations and lower iron oxyhydroxide activity. As a result, as pH increases, less OH• was produced, which led to a decline in iron ions. At a neutral or higher pH, the soluble Fe^{2+} easily precipitated with the Fe^{3+} oxyhydroxides. However, $[Fe(H_2O)_6]^{2+}$, a Fe-complex molecule, was generated at a

very low pH value of 2, prohibiting Fe(II) from interacting with H_2O_2, (Wardman and Candeias, 1996). Additionally, at low pH circumstances, the hydroxyl species rapidly diminished when H^+ was coupled with OH•, suppressing the deterioration of AY (Equation 2). The electro-Fenton degradation of Acid Red 18 dye revealed that raising the pH from 2 to 3 had slightly increased the dye's degradation; however, when further increased the pH up to 9, the dye's degradation was significantly suppressed (Malakootian and Moridi, 2017). Therefore, the optimum pH range was above 2 and 3.

3.3.2 Optimization of H_2O_2 and Solid Catalyst Dosage

The hydrogen peroxide (H_2O_2) dosage was crucial to optimize the Fenton-like reaction efficiently, meaning that an optimized dosage could maximize the AY's percentage degradation. Therefore, several studies were carried out at the pH of 3, using a constant nanocatalyst dosage of 120 mg/L and various H_2O_2 dosages from 0.06 to 0.14 mL/L in a dark environment. Figure 4(a) depicts the AY's acquired and observed H_2O_2 dose-dependent degradation efficiency. The graph ascertained that the AY breakdown percentage was improved from 84.36 to 93.54%, raising the dosage of hydrogen peroxide (30.0% v/v) from 0.06 to 0.1 mL/L. However, a further increase in the H_2O_2 dosage, from 0.1 to 0.14 mL/L, decreased the rate from 93.54 to 85.15%. Higher concentrations of H_2O_2 react with excess OH• to produce water molecules and the hydroperoxyl radical (HO_2•) (*Cf* Eq. 3), which saturates the amount of OH• available for the oxidation process, so-called "OH radical scavenger" (Kim et al., 2009; 2010). Additionally, Fida (Fida et al., 2017b) described the behaviour of OH• being quenched by •HO_2 (Eq. 4). Organic molecules were slowly degraded due to the radical species' rapid dissipation. The findings support the Fenton-like removal of naproxen utilizing a nanocomposite of goethite and montmorillonite (Paul et al., 2011).

$$H_2O_2 + HO\bullet \rightarrow H_2O + HOO\bullet \quad (3)$$

$$HOO\bullet + HO\bullet \rightarrow H_2O + O_2 \quad (4)$$

In addition, the impact of the nanocatalyst Fe^0-Ag^0@BN dosage (80 to 160 mg/L) was evaluated in regard with the AY degradation (*Cf*, Fig. 3(b)). Under dark circumstances, the AY (2 mg/L) solution at the pH of 3 and the H_2O_2 concentration (0.1 mL/L), the AY degradation was performed at a wide range of catalyst dosages. The results revealed that the AY degradation

reached its maximum level at a solid catalyst dosage of 120 mg/L. Therefore, for further investigations, a catalyst amount of 120 mg/L can be used as most optimum dosage. The AY was decomposed at higher nanocatalyst contents since it provided relatively more chemically active sites to adsorb the pollutant molecules, which was well described in terms of 3-D crosslinked structure with more functional sites (Kim et al., 2005; 2012). However, a significantly higher catalyst dosage scavenged the formation of hydroxyl radical (Equation 5) by suppressing the AY degradation (Hassan and Hameed, 2011). The breakdown of naproxen employing a nanocomposite of modified iron oxyhydroxide nanoparticles over montmorillonite clay (MGO) showed a similar degradation pattern (Sétifi et al., 2019).

$$Fe^{2+} + HO\bullet \rightarrow Fe^{3+} + HO^{-} \qquad (5)$$

3.3.3 Impact of Photo Illumination on AY Degradation

The consequences of utilizing various lighting sources (UV-A and LED-Vis) were examined for the Fenton-like reaction. Figure 5(a) clearly ascertained that the photo illumination evidently accelerated the degradation of AY. The UV-A illumination relatively achieved a higher degradation of AY, when compared to the LED illumination in the photo-Fenton-like processes. In Fig. 5, the most optimum time dependence was determined for the highest AY degradation under different reaction conditions. The combined treatment of the Fenton-like degradation of AY by Fe^0-Ag^0@BN, employing the UV-A and LED-Vis illuminations for 30 and 60 min, achieved an efficiency of 100 %. However, 93 % of AY degradation in dark conditions was made in 2 h.

Similarly, the degradation efficiency for AY utilizing the Fe^0@BN nanocatalyst was 79.56 % in the dark. The comparative results indicated that adding Ag(NPs) considerably improved the catalyst's efficiency in degrading AY in the light-illuminated Fenton-like process. The illumination of LED-Vis light degraded a significant amount of the AY, allowing a potential use of the nanocatalyst composite in visible-light-driven reactor operations. Moreover, light illumination substantially accelerated the production of •OH radicals by adding up a synergistic effect on the AY degradation (Eq. 6) (Sapach and Viraraghavan, 1997). The presence of Ag(NPs) synergized the formation of HO• in the reaction medium, hence, it

favoured the degradation of AY (He et al., 2014). In other words, the more active sites on the surface of the nanocatalyst composite enhanced the photocatalytic activities. Furthermore, as seen in Eq. 7, the light energy improved both the catalytic performance of the Fe that leached out of the nanocomposite and the photolysis of H_2O_2 (Sétifi et al., 2019; Kim et al., 2010).

$$H_2O_2 \xrightarrow{hv} 2HO\bullet \qquad (6)$$

$$\text{Fe(III)} + H_2O + hv \rightarrow Fe(II) + HO\bullet + H^+ \qquad (7)$$

3.3.4 Concentration Dependence Removal

The experimental investigation determined the impact of the preliminary pollutant concentration on the percentage degradation of the target pollutant molecules. Figure 5(b) represented the AY degradation at varied concentrations of AY (from 2 to 30 mg/L) under the photo-Fenton-like process. In both dark and photo-illuminated Fenton-like reactions, increasing the initial concentration caused a significant reduction in the AY degradation. In terms of values, for the Fenton-like reaction, the percentage elimination of AY was decreased from 100 to 82 %, when the AY concentration was increased from 2 to 30 mg/L under the UV-A irradiation. In comparison, the degradation rate declined from 100 to 68 % in the LED-Vis irradiation for a similar increase in the AY concentration. The steady diminution in degradation with a rise in AY concentration was explained by the fact that at higher pollutant concentrations, the extent of oxidant species, i.e., the quantity of HO• radicals, is less to degrade a large number of the AY species in aqueous solutions. With the lower AY concentration, a correspondingly greater number of active sites are accessible for the contaminants to bind to the catalyst surface. As a result, AY molecules are available at the catalyst surface and efficiently undergo the degradation process.

Alternatively, at the higher AY concentrations, comparatively fewer active sites at the catalyst's surface are available for many more pollutant molecules, hence, causing a decrease in the degradation efficiency of AY. Moreover, the AY molecules occupied more active sites on the nanocatalyst surface at the higher concentrations, thereby lessening the leaching of Fe

into the reaction mixture. In other words, it diminished the generation of HO• radicals, which in turn decreased the AY degradation.

3.3.5 Kinetic Studies for AY Degradation

Fenton or Fenton-like processes include several steps that are all compatible with a particular group of rate constants. The AY degradation data can be explained by the pseudo-first-order (PFO) and/or pseudo-second-order (PSO) rate equations (Gopal et al., 2020). Figure 6 demonstrates the fitting results of the experimental data and model data. The rate constants (k_f) and R^2 values for the AY degradation, utilizing the Fe^0-Ag^0@BN were obtained and found to be 0.0286 min^{-1} and 0.5183 min^{-1}, respectively. Similarly, the PSO kinetic representation's reaction rate constants (k_s) and R^2 value were 0.0596 $Lmin^{-1}mg^{-1}$ and 0.9702 $Lmin^{-1}mg^{-1}$, respectively. The results infer that the AY degradation in the photo-Fenton-like process apparently followed the pseudo-second-order rate kinetics.

3.3.6 Influence of Cations/Anions on AY Degradation

Cations and anions often coexist in natural wastewater streams. Therefore, to correlate the degradation of AY in actual matrix samples, the presence of several coexisting ions, including cations like Pb^{2+}, Cd^{2+}, Cu^{2+}, and Ni^{2+}, and anions like PO_4^{3-}, $C_2H_5NO_2$, $C_2O_4^{2-}$, and SO_4^{2-}, were investigated in terms of the degradation of AY under optimized reaction conditions. The cation or anion concentration remained stable at 10 mg/L with an AY concentration of 2 mg/L. Figure 7(a) illustrated the influence of various cations and anions on the AY degradation. Because the positively charged metal ions had a lower affinity towards the Fe^0-Ag^0@BN nanocatalyst surface, which functions positively under acidic pH conditions, the presence of Pb^{2+}, Cd^{2+}, Cu^{2+}, and Ni^{2+} was essentially minimal. However, the presence of anions had a more noticeable impact on the degradation of AY. The anions predominantly hindered the catalyst active sites of the AY by preventing pollutant molecules from being eliminated.

Additionally, specific ions and molecules such as SO_4^{2-}, were found to be more efficient in quenching the h^+/HO• (Lalliansanga et al., 2020). Most anions interact with the dissolved Fe^{3+}/Fe^{2+} and Ag^+ from the catalysts to form complexes. As a result, they lessen the production of •OH, thus lowering the AY degradation efficiency.

3.3.7 Degradation of AY

The studies determined the percentage of the AY degradation, using the Fe^0-Ag^0@BN nano-catalyst under the UV-A & LED-Vis illuminations. The non-purgeable organic carbon (NPOC)

data collected for the AY solutions both before and after treatment were utilized to determine the percentage of the AY degradation in the photo-Fenton-like reaction.

Figure 7(b) shows AY's degradation percentage (%) at various AY concentrations. The findings show that AY mineralizes significantly in the Fenton-like process. Increasing the AY concentration from 2 to 30 mg/L triggered an apparent reduction in the mineralization from 98.46 to 76.46 % under UV-A irradiation. Similarly, AY mineralization decreased from 91 to 52 % under LED-Vis illumination with the same increase in AY concentration. According to Feng (Feng et al., 2005), mineralization of the Orange-II dye (0.2 mM), when combined with clay bentonite-supported nZVI, 10.0 mM H_2O_2, and UV-C light (8W), varies from 50 to 60 %. Similar to this, Lalliansanga (Lalliansanga et al., 2022) used an Ag(NPs)/TiO_2 thin film and found 48.36 % mineralization of AY (1.0 mg/L) for 2 h of UV-A irradiation. Such results demonstrated that the catalyst Fe^0-Ag^0@BN appeared to be efficient for the significant elimination of AY (2 mg/L) under the UV-A and LED-visible irradiations.

3.3.8 Radical Scavengers Study

The involvement of HO• in the degradation route of AY, the investigation should be expanded by incorporating a few well-known radical quenchers for HO• such as HCO_3^- and isopropanol (Lalliansanga et al., 2022). Another essential reactive oxygen radical, the $\bullet O_2^-$, which combines with oxygen and photo-generated holes (h^+) to make singlet oxygen, is quenched with NaN_3 (sodium azide). The organic molecules in aqueous media are very reactive to this singlet oxygen (Barrios et al., 2021). Hence, the AY degradation at 2 mg/L (100 mL) when confronted with free-radical quenchers, i.e., isopropanol, sodium bicarbonate, and sodium azide, at 0.1 $molL^{-1}$ (1.0 mL) was studied in a photo-assisted Fenton-like reaction. Figure 8 well demonstrated that the presence of radical quenchers significantly suppressed the AY degradation rate. The degradation of AY decreased from 98 % to 35 % to 15 % in the presence of such quenchers, which signifies that the principal involvement of the HO• radical was the limiting factor of the degradation process. The photocatalytic removal of AY, using gold and silver nanoparticles [(Au-NPs)/(Ag(NPs)] modified nanocomposites with titanium dioxide proceeded through the HO• and $\bullet O_2^-$ radicals induced degradation mechanisms (Lalliansanga et al., 2020; Lalliansanga et al., 2022). Similar results were obtained by Hofmann and Andrew (Hofmann and Andrews, 2006), using the bicarbonate quenchers that made the HO•. HCO_3^- to transform the HO• to less active hydroxyl ions, which prevents the production of BrO_3^-. Thus, the engagement of HO• and $\bullet O_2^-$ radicals was the primary mechanism for the AY degradation. The results also indicated that HCO_3^- and NaN_3 significantly suppressed the AY degradation.

3.3.9 Leaching of Fe(II)

The interactions between Fe(II) and H_2O_2 generate the HO• reactive radicals in solution, and the HO• radicals degrade the pollutant molecules in aqueous solution. As the reaction progresses, the amount of Fe^{2+} increases, and more HO• is generated simultaneously. The presence of H_2O_2 in conjunction with a nanocatalyst is the process's primary generator of reactive oxygen species (ROS). The average active sites available at the catalyst surface and their affinity for H_2O_2 are the driving force that controls the breakdown of H_2O_2. Additionally, Fe^0@BN exhibits lower Fe(II) leaching than bare iron nanoparticles. Therefore, using only Fe(NPs) leads to a secondary contamination. At an optimum reaction condition, the Fe^0-Ag^0@BN was employed to observe the Fe(II) leaching in the degradation of 2 mg/L of AY for a 2 h reaction time. The total concentration of 70 µg/L of Fe(II) leached out at the end of the reaction in Fig. 7(a). The results demonstrated that a minimum of iron leached out from the catalyst Fe^0-Ag^0@BN and implied that the catalyst might be advantageous in the photo-Fenton-like process. Figure 7(a) also displays the C_t/C_0 values for degrading AY. The AY degradation throughout reaction time was inversely associated with the iron leaching, so the degradation of AY increased with increasing iron leaching.

3.3.10 Reusability Test

The ability to recycle of catalyst is connected with the stability of the catalyst. The reusability test of the material was conducted, and concluded that the nanocatalyst had a high potential for practical applications. The nanocatalyst's capacity to employ the photo-Fenton-like process was dependent on its stability, which is quite essential for the practical value of the technology. The nanocatalyst should be usable for a relatively long-term application. Therefore, the Fe^0-Ag^0@BN nanocatalyst was tested and confirmed in terms of evaluating the reusability and stability (or durability) while removing AY. Figure 8(b) shows the consistency of reusing the Fe^0-Ag^0@BN nanocatalyst for the degradation of AY. Under the UV-A irradiation, while keeping optimum reaction conditions, the degradation efficiency was presented. The findings demonstrated that the degradation percentage of AY slightly decreased with each consecutive cycle of experiments.

Moreover, after the fifth cycle of the experiment, the degradation efficiency only decreased from 100 to 95%. The decrease in the AY removal efficiency was minimal, even after the 5 experimental cycles. This indicates that the bimetallic nanocatalyst is promising for long-term applications in the photo-assisted Fenton-like reaction. Previously, the Fenton-like

methylene blue degradation, employing a copper nanocatalyst supported by bentonite, demonstrated that the copper nanocatalyst showed a high stability (Issaabadi et al., 2017). The supporting materials, *viz*., bentonite, charcoal, graphite, impart the nanocatalyst reasonable stability by permitting only a limited amount of leaching of the nanoparticles from the catalyst surface (Dihingia and Tiwari, 2022b).

3.3.11 Degradation Efficiency in Natural Water Samples

The use of the Fe^0-Ag^0@BN nanocatalyst was assessed in terms of removing AY from the natural water samples. It provides potential ramifications that allow this technology to be implemented for much wider applications. Additionally, this study can help evaluate the appropriateness and selectivity of nanocatalyst for real applications.

Physicochemical studies of the natural water samples W1 and W2 were performed (Table 2). Both samples had low concentrations of Fe, Cu, Ni, Pb, Mn, and Zn. However, the level of calcium was relatively high in the water samples. The NPOC values were at moderate levels. However, the inorganic carbon content was relatively high in both samples. The sulphate, nitrate, and phosphate concentrations in both samples were low as well. Different AY concentrations (2, 4, and 6 mg/L) were spiked with water samples (W1 and W2) at a pH of 3. Using the Fe^0-Ag^0@BN nanocatalyst, AY's photo-assisted Fenton-like degradation experiments were conducted for 2 h, irradiating the samples separately with UV-A and LED-Visible lights, respectively. Figure 9(b) shows the percentage degradation of AY at varied AY concentrations for the water samples of W1 and W2, and the distilled/deionized (D/D) water. The results inferred that a minimal decrease in the percentage degradation of AY occurred for the W1 and W2 samples, compared to the D/D water for both the UV-A and LED-light-assisted Fenton-like processes. The findings demonstrated the capability of the new nanocatalyst in removing AY from natural water bodies with high efficiency, using photo-assisted Fenton-like reactions.

4. Conclusion

Through a straightforward and environmentally friendly process, the bentonite-supported bimetallic Fe^0-Ag^0@BN nanocatalyst was successfully synthesized. Bentonite, Fe^0@BN, and Fe^0-Ag^0@BN had band gap energies of 3.26, 2.24, and 2.16 eV, respectively, according to the DRS measurements. Under a dark environment, the Fenton-like reactions demonstrated 93.5%

of degradation for AY (2 mg/L) at the pH of 3 and 120 mg/L of Fe^0-Ag^0@BN nanocatalyst dosage, and 0.1 mL/L of H_2O_2 (30 %) at 120 min reaction time. Additionally, light exposures greatly enhanced the degradation rate of AY. Since •OH radicals play a major role in the AY degradation process, the UV-A light facilitated the degradation up to 98 %. The nanocatalyst showed quite high stability and durability with 5 times of reusability, still keeping over 95 % degradation rate of AY. Also, the efficiency of AY degradation remained almost unchanged for testing actual water samples. This study introduced a novel and greener bimetallic nanocatalyst Fe^0-Ag^0@BN to remove recalcitrants, including AY in an aqueous solution with the aid of the advanced Fenton-like process.

Declarations

Ethical Approval

(applicable for both human and/ or animal studies. Ethical committees, Internal Review Boards and guidelines followed must be named. When applicable, additional headings with statements on consent to participate and consent to publish are also required)

"Not Applicable."

Funding

(details of any funding received)

"Not Applicable."

Availability of data and materials

(a statement on how any datasets used can be accessed)

"Not Applicable."

Conflict of Interests

The authors declare that they have no conflict of interest.

References

Adlnasab, L., Shabanian, M., Ezoddin, M., & Maghsodi, A., 2017. Amine-rich functionalized mesoporous silica for the effective removal of alizarin yellow and phenol red dyes from wastewaters based on response surface methodology. Materials Science and Engineering: B, 226, 188–198. https://doi.org/10.1016/j.mseb.2017.09.017

Banat, F. A., Al-Bashir, B., Al-Asheh, S., & Hayajneh, O., 2000. Adsorption of phenol by bentonite. Environ. Pollut. 107(3), 391–398. https://doi.org/10.1016/S0269-7491(99)00173-6

Barrios, B., Mohrhardt, B., Doskey, P. V., & Minakata, D., 2021. Mechanistic Insight into the Reactivities of Aqueous-Phase Singlet Oxygen with Organic Compounds. Environ. Sci. Technol. 55(12), 8054–8067. https://doi.org/10.1021/acs.est.1c01712

Bounab, L., Draoui, K., Ahrouch, M., Hadri, M., Bouchta, D., & Barhoun, A., 2017. An effective functionalized Moroccan bentonite: Application for a green remediation of m-Cresol, J. Mater. Environ. Sci. 8(1):244-256

Chandraker, S. K., Lal, M., Ghosh, M. K., Tiwari, V., Ghorai, T. K., & Shukla, R., 2020. Green synthesis of copper nanoparticles using leaf extract of Ageratum houstonianum Mill. and study of their photocatalytic and antibacterial activities. Nano Express, 1(1), 010033. https://doi.org/10.1088/2632-959X/ab8e99

Dihingia, H., & Tiwari, D., 2022a. Green synthesis of bimetallic nanocomposite: Efficient use of nanocomposite in the removal of phenol and n-(n-Propyl) thiourea by photo-Fenton-like process. J. Cleaner Product. 374. https://doi.org/10.1016/j.jclepro.2022.133913

Dihingia, H., & Tiwari, D., 2022b. Impact and implications of nanocatalyst in the Fenton-like processes for remediation of aquatic environment contaminated with micro-pollutants: A critical review. J. Wat. Proc. Eng. 45, 102500. https://doi.org/10.1016/j.jwpe.2021.102500

Djellabi, R., Su, P., Elimian, E. A., Poliukhova, V., Nouacer, S., Abdelhafeez, I. A., et al., 2022. Advances in photocatalytic reduction of hexavalent chromium: From fundamental concepts to materials design and technology challenges. J. Wat. Proc. Eng. 50, 103301. https://doi.org/10.1016/j.jwpe.2022.103301

dos Santos, A. B., Cervantes, F. J., & van Lier, J. B., 2007. Review paper on current technologies for decolourization of textile wastewaters: perspectives for anaerobic biotechnology. Biores. Technol. 98(12), 2369–2385. https://doi.org/10.1016/j.biortech.2006.11.013

Feng, J., Hu, X., & Yue, P. L., 2005. Discoloration and mineralization of Orange II by using a bentonite clay-based Fe nanocomposite film as a heterogeneous photo-Fenton catalyst. Water Res. 39(1), 89–96. https://doi.org/10.1016/j.watres.2004.08.037

Fida, H., Zhang, G., Guo, S., & Naeem, A., 2017a. Heterogeneous Fenton degradation of organic dyes in batch and fixed bed using La-Fe montmorillonite as catalyst. J. Colloid Interface Sci. 490, 859–868. https://doi.org/10.1016/j.jcis.2016.11.085

Fida, H., Zhang, G., Guo, S., & Naeem, A., 2017b. Heterogeneous Fenton degradation of organic dyes in batch and fixed bed using La-Fe montmorillonite as catalyst. J. Colloid Interface Sci. 490, 859–868. https://doi.org/10.1016/j.jcis.2016.11.085

Flores, Y., Flores, R., & Gallegos, A. A., 2008. Heterogeneous catalysis in the Fenton-type system reactive black 5/H2O2. J. Molecular Cat. A. 281(1–2), 184–191. https://doi.org/10.1016/j.molcata.2007.10.019

Gopal, G., Sankar, H., Natarajan, C., & Mukherjee, A., 2020. Tetracycline removal using green synthesized bimetallic nZVI-Cu and bentonite supported green nZVI-Cu nanocomposite: A comparative study. J. Environ. Manage. 254, 109812. https://doi.org/10.1016/j.jenvman.2019.109812

Guo, T., Wang, K., Zhang, G., & Wu, X.. 2019. A novel α-Fe2O3@g-C3N4 catalyst: Synthesis derived from Fe-based MOF and its superior photo-Fenton performance. Appl. Surface Sci. 469, 331–339. https://doi.org/10.1016/j.apsusc.2018.10.183

Hassan, H., & Hameed, B. H., 2011. Fenton-like Oxidation of Acid Red 1 Solutions Using Heterogeneous Catalyst Based on Ball Clay. Inter. J. Environ. Sci. Develop. 218–222. https://doi.org/10.7763/IJESD.2011.V2.127

He, D., Miller, C. J., & Waite, T. D., 2014a. Fenton-like zero-valent silver nanoparticle-mediated hydroxyl radical production. J. Cat. 317, 198–205. https://doi.org/10.1016/j.jcat.2014.06.016

Herney-Ramirez, J., Vicente, M. A., & Madeira, L. M., 2010a. Heterogeneous photo-Fenton oxidation with pillared clay-based catalysts for wastewater treatment: A review. Appl. Cat. B. 98(1–2), 10–26. https://doi.org/10.1016/j.apcatb.2010.05.004

Hofmann, R., & Andrews, R. C., 2006. Impact of H_2O_2 and (bi)carbonate alkalinity on ammonia's inhibition of bromate formation. Water Res. 40(18), 3343–3348. https://doi.org/10.1016/j.watres.2006.07.032

Issaabadi, Z., Nasrollahzadeh, M., & Sajadi, S. M., 2017. Green synthesis of the copper nanoparticles supported on bentonite and investigation of its catalytic activity. J. Cleaner Prod. 142, 3584–3591. https://doi.org/10.1016/j.jclepro.2016.10.109

Kecić, V., Kerkez, Đ., Prica, M., Lužanin, O., Bečelić-Tomin, M., Pilipović, D. T., & Dalmacija, B., 2018. Optimization of azo printing dye removal with oak leaves-nZVI/H2O2 system using statistically designed experiment. J. Cleaner Prod. 202, 65–80. https://doi.org/10.1016/j.jclepro.2018.08.117

Kim, D. I., Petrisor, I. G., Yen, T. F. (2005) Evaluation of biopolymer-modified concrete systems for disposal of cathode ray tube glass. Journal of Air & Waste Management, 55, 961-969.

Kim, D. I, Chen, J. R., Yen, T. F. (2009) Mechanism and kinetics of reductive dehalogenation of PBB (polybrominated biphenyl) in the sonolytic and ketyl radical system. *Journal of Hazardous Materials*, 163: 231-238.

Kim, D. I, Chen, J. K., Yen, T. F. (2010) Mechanism of naval derusting wastewater containing high concentration of iron, treated in UV photo-Fenton oxidation. *Journal of Environmental Sciences,* 22(7) 991-997.

Kim, D. I., Park, J. S., Yen, T. F. (2012). Feasibility study on cross-linked biopolymeric

concrete encapsulating selenium glass wastes. J*ournal of Air & Waste Management,* 62(8), 898-904. https://doi.org/10.1080/10962247.2012.675939

Kumar, G., & Dutta, R. K., 2022. Sunlight mediated photo-Fenton degradation of tetracycline antibiotic and methylene blue dye in aqueous medium using FeWO4/Bi2MoO6 nanocomposite. Pro. Safety Environ. Protec. 159, 862–873. https://doi.org/10.1016/j.psep.2022.01.063

Lalliansanga, Tiwari, D., Tiwari, A., Shukla, A., Kim, D.-J., Yoon, Y.-Y., & Lee, S.-M., 2020a. Facile synthesis and characterization of nanocomposite Au0(NPs)/titanium dioxide: Photocatalytic degradation of Alizarin Yellow. J. Ind. Eng. Chem. 82, 153–163. https://doi.org/10.1016/j.jiec.2019.10.008

Lalliansanga, Tiwari, D., Tiwari, A., Shukla, A., Shim, M. J., & Lee, S.-M., 2022. Facile synthesis and characterization of Ag(NP)/TiO2 nanocomposite: Photocatalytic efficiency of catalyst for oxidative removal of Alizarin Yellow. Cat. Today S0920586120306490. https://doi.org/10.1016/j.cattod.2020.09.010

Liang, B., Yao, Q., Cheng, H., Gao, S., Kong, F., Cui, D., et al., 2012. Enhanced degradation of azo dye alizarin yellow R in a combined process of iron–carbon microelectrolysis and aerobic bio-contact oxidation. Environ. Sci Pollut. Res. 19(5), 1385–1391. https://doi.org/10.1007/s11356-012-0785-4

Lin, C.-C., & Hsu, S.-T., 2018. Performance of nZVI/H2O2 process in degrading polyvinyl alcohol in aqueous solutions. Sep. Purif. Technol. 203, 111–116. https://doi.org/10.1016/j.seppur.2018.03.041

Liou, R.-M., Chen, S.-H., Hung, M.-Y., Hsu, C.-S., & Lai, J.-Y., 2005. Fe (III) supported on resin as effective catalyst for the heterogeneous oxidation of phenol in aqueous solution. Chemosphere 59(1), 117–125. https://doi.org/10.1016/j.chemosphere.2004.09.080

Malakootian, M., & Moridi, A., 2017. Efficiency of electro-Fenton process in removing Acid Red 18 dye from aqueous solutions. Pro. Safety Environ. Protec. 111, 138–147. https://doi.org/10.1016/j.psep.2017.06.008

Marimuthu, S., Antonisamy, A. J., Malayandi, S., Rajendran, K., Tsai, P.-C., Pugazhendhi, A., & Ponnusamy, V. K., 2020. Silver nanoparticles in dye effluent treatment: A review on synthesis, treatment methods, mechanisms, photocatalytic degradation, toxic effects and mitigation of toxicity. J. Photochem. Photobio. B. 205, 111823. https://doi.org/10.1016/j.jphotobiol.2020.111823

Midik Ertosun, F., Cellat, K., Eren, O., Gül, Ş., Kuşvuran, E., & Şen, F., 2019. Comparison of nanoscale zero-valent iron, fenton, and photo-fenton processes for degradation of pesticide 2,4-dichlorophenoxyacetic acid in aqueous solution. SN Appl. Sci. 1(11), 1491. https://doi.org/10.1007/s42452-019-1554-5

Ogugbue, C. J., & Sawidis, T., 2011. Bioremediation and Detoxification of Synthetic Wastewater Containing Triarylmethane Dyes by Aeromonas hydrophila Isolated from Industrial Effluent. Biotechnol. Res. Inter. 2011, e967925. https://doi.org/10.4061/2011/967925

Paul, B., Martens, W. N., & Frost, R. L., 2011. Organosilane grafted acid-activated beidellite clay for the removal of non-ionic alachlor and anionic imazaquin. Appl. Surf. Sci. 257(13), 5552–5558. https://doi.org/10.1016/j.apsusc.2011.01.034

Pera-Titus, M., García-Molina, V., Baños, M. A., Giménez, J., & Esplugas, S., 2004. Degradation of chlorophenols by means of advanced oxidation processes: a general review. Appl. Cat. B. 47(4), 219–256. https://doi.org/10.1016/j.apcatb.2003.09.010

Prieto, P., Nistor, V., Nouneh, K., Oyama, M., Abd-Lefdil, M., & Díaz, R., 2012. XPS study of silver, nickel and bimetallic silver–nickel nanoparticles prepared by seed-mediated growth. Appl. Surf. Sci. 258(22), 8807–8813. https://doi.org/10.1016/j.apsusc.2012.05.095

Przystaś, W., Zabłocka-Godlewska, E., & Grabińska-Sota, E., 2012. Biological Removal of Azo and Triphenylmethane Dyes and Toxicity of Process By-Products. Wat. Air Soil Poll. 223(4), 1581–1592. https://doi.org/10.1007/s11270-011-0966-7

699 Ramirez, J. H., Maldonado-Hódar, F. J., Pérez-Cadenas, A. F., Moreno-Castilla, C., Costa, C.
700 A., & Madeira, L. M., 2007. Azo-dye Orange II degradation by heterogeneous Fenton-like
701 reaction using carbon-Fe catalysts. Appl. Cat. B. 75(3–4), 312–323.
702 https://doi.org/10.1016/j.apcatb.2007.05.003
703
704 Rodney, John. D., Deepapriya, S., Annie Vinosha, P., Krishnan, S., Janet Priscilla, S., Daniel,
705 R., & Jerome Das, S., 2018. Photo-Fenton degradation of nano-structured La doped CuO
706 nanoparticles synthesized by combustion technique. Optik 161, 204–216.
707 https://doi.org/10.1016/j.ijleo.2018.01.125
708
709 Sapach, R., & Viraraghavan, T., 1997. An introduction to the use of hydrogen peroxide and
710 ultraviolet radiation: An advanced oxidation process. J. Environ. Sci. Health Part A. 32(8),
711 2355–2366. https://doi.org/10.1080/10934529709376686
712
713 Sétifi, N., Debbache, N., Sehili, T., & Halimi, O., 2019. Heterogeneous Fenton-like oxidation
714 of naproxen using synthesized goethite-montmorillonite nanocomposite. J. Photochem.
715 Photobio. A. 370, 67–74. https://doi.org/10.1016/j.jphotochem.2018.10.033
716
717 Sulaiman, S., & Al-Jabari, M., 2021. Enhanced adsorptive removal of diclofenac sodium
718 from aqueous solution by bentonite- supported nanoscale zero-valent iron. Arab J. Basic
719 Appl. Sci. 28, 51–63. https://doi.org/10.1080/25765299.2021.1878655
720
721 Tahir, M. B., Sohaib, M., Sagir, M., & Rafique, M., 2020. Role of Nanotechnology in
722 Photocatalysis. Ref. Module Mat. Sci. Mat. Eng. B978-0-12-815732-9.00006–1.
723 https://doi.org/10.1016/B978-0-12-815732-9.00006-1
724
725 Ulucan-Altuntas, K., & Kuzu, S. L., 2019. Modelling and optimization of dye removal by
726 Fe/Cu bimetallic nanoparticles coated with different Cu ratios. Mat. Res. Exp. 6(11), 1150a4.
727 https://doi.org/10.1088/2053-1591/ab4bb5
728 Wang, C., Sun, R., & Huang, R., 2021. Highly dispersed iron-doped biochar derived from
729 sawdust for Fenton-like degradation of toxic dyes. J. Clean. Prod. 297, 126681.
730 https://doi.org/10.1016/j.jclepro.2021.126681
731

Wardman, P., & Candeias, L. P., 1996. Fenton Chemistry: An Introduction. Rad. Res. 145(5), 523–531. https://doi.org/10.2307/3579270

Yamaguchi, R., Kurosu, S., Suzuki, M., & Kawase, Y., 2018. Hydroxyl radical generation by zero-valent iron/Cu (ZVI/Cu) bimetallic catalyst in wastewater treatment: Heterogeneous Fenton/Fenton-like reactions by Fenton reagents formed in-situ under oxic conditions. Chem. Eng. J. 334, 1537–1549. https://doi.org/10.1016/j.cej.2017.10.154

Ye, J., Luo, Y., Sun, J., & Shi, J., 2021. Nanoscale Zero-Valent Iron Modified by Bentonite with Enhanced Cr(VI) Removal Efficiency, Improved Mobility, and Reduced Toxicity. Nanomaterials 11, 2580. https://doi.org/10.3390/nano11102580

Zhan, H., Zhou, Q., Li, M., Zhou, R., Mao, Y., & Wang, P., 2022. Photocatalytic O2 activation and reactive oxygen species evolution by surface B-N bond for organic pollutants degradation. Appl. Cat. B. 310, 121329. https://doi.org/10.1016/j.apcatb.2022.121329

Zhang, M.-H., Dong, H., Zhao, L., Wang, D.-X., & Meng, D., 2019. A review on Fenton process for organic wastewater treatment based on optimization perspective. Sci. Total Environ. 670, 110–121. https://doi.org/10.1016/j.scitotenv.2019.03.180

List of Tables

Table 1

Qualitative identification of various phytochemicals present in *P. Guajava* leaf extract

Sample No.	Phytochemicals	Test	Result
1	Alkaloids	Mayer's test, Wagner test	Positive
2	Flavonoids	Ferric chloride test, lead acetate test	Positive
3	Tannins	Ferric chloride test	Positive
4	Phlobatannins	HCl test	Negative
5	Triterpenes	Salkowski test, Liberman test	Positive
6	Diterpenes	Copper acetate test	Positive
7	Steroids	Salkowski test	Positive
8	Saponins	Foam test	Negative
9	Cardiac glycoside	Keller Killani test	Positive

Table 2

Physicochemical properties of two real water samples

Source	GPS location	TOC (mg/L)	Cations (mg/L)	Anions	Physical properties
W_1	*Latitude* = 23°44'3"N *Longitude* = 92°40'33"E *Elevation* = 833 m	*NPOC*=1.349 *TC* = 18.851 *IC* = 17.502	*Cu* = 0.0036 *Ca* = 2.3582 *Zn* = 0 *Pb*= 0.0752 *Ni* = 0.0195 *Fe* = 0 *Mn* = 0	*Sulphate* = 11 mg/L *Phosphate*= 0.1 mg/L *Nitrate* = 9 µg/L	*pH* = 8.21 *Salinity* = 0.1 PSU *Oxd. & red. Potential* = 160.7 mV *Resistivity* = 0.0045 $M\Omega cm^{-1}$ *Conductivity* = 199 μScm^{-1} *TDS* = 100 ppm
W_2	Latitude = 23°44'16"N Longitude = 92°40'10"E Elevation = 884 m	*NPOC*=0.976 *TC* = 8.443 *IC* = 7.466	*Cu* = 0.01 *Ca* = 3.4589 *Zn* = 0.0054 *Pb*= 0.0442 *Ni* = 0.0239 *Fe* = 0 *Mn* = 0	*Sulphate* = 7 mg/L *Phosphate* = 0.1 mg/L *Nitrate* = 20 µg/L	*pH* = 7.9 *Salinity* = 0.07 PSU *Oxd. & red. Potential* = 194.5mV *Resistivity* = 0.0078 $M\Omega cm^{-1}$ *Conductivity* = 129 μScm^{-1} *TDS* = 65 ppm

List of Figures

Fig. 1 The SEM images of (a) BN, (b) Fe^0@BN, and (c) Fe^0-Ag^0@BN solids, the EDX spectroscopic representation of (d) BN, (e) Fe^0@BN, and (f) Fe^0-Ag^0@BN, the TEM images of (g) Fe^0@BN, and (h) Fe^0-Ag^0@BN nanocomposite solids

Fig. 2 Tauc plots of bentonite (BN), Fe^0@BN, and Fe^0-Ag^0@BN solids for determining intermediate band-gap energy (E_g); (b) N_2 adsorption-desorption isotherms obtained for pristine (BN), Fe^0@BN, and Fe^0-Ag^0@BN nanocomposites; and (c) the pore size distribution for the pristine bentonite (BN), Fe^0@BN, and Fe^0-Ag^0@BN nanocomposites; (d) XRD pattern of BN and nanocomposite solids [Inset: The XRD spectra of Fe^0-Ag^0@BN nanocomposite material].

Fig. 3 The XPS spectroscopic analysis for the Fe0-Ag0@BN solids [Inset: XPS pattern of Fe and Ag in the Fe0-Ag0@BN nanocatayst]

Fig. 4 Degradation percentage (%) of AY at different initial solution pH values [nanocatalyst dosage = 120 mg/L, H_2O_2 dosage (30 %) = 0.1 mL/L, AY = 2.0 mg/L, duration time = 2 h] under dark conditions [(a) Degradation of AY in the different dosages (0.06 to 0.14 mL/L) of H_2O_2 in the dark environment and (b) Degradation of AY at various dosages of Fe0-Ag0@BN in the dark environment]

Fig. 5 (a) Degradation of AY vs. reaction time (min) in different reaction conditions [pH = 3.0, AY = 2.0 mg/L, nanocatalyst dosage = 120 mg/L, H_2O_2 dosage = 0.1 mL/L, reaction time = 120 min], (b) Influence of initial pollutant's concentration on the AY degradation under different illuminations [pH = 3.0, nanocatalyst dosage = 120.0 mg/L, H_2O_2 dosage = 0.1 mL/L, reaction time = 120 min]

Fig. 6 The kinetics models of AY degradation, using (a) the PFO; and (b) PSO

Fig. 7 (a) Impact of co-existing cations and anions in the photo-assisted Fenton-like degradation of Alizarin Yellow [pH = 3.0, AY = 2.0 mg/L, co-ions = 10.0 mg/L nanocatalyst dosage = 120 mg/L H_2O_2 dosage = 0.1 mL/L reaction duration = 120 min];, (b) Degradation (%) of AY at different concentrations [pH = 3.0, nanocatalyst dosage = 120.0 mg/L, H_2O_2 dosage = 0.1 mL/L, reaction duration = 120 min]

Fig. 8 (a) Impact in degradation (%) of AY in the presence of scavengers [pH = 3.0; AY = 2 mg/L; [scavenger]: 0.1 $molL^{-1}$ (1.0 mLL^{-1}); catalyst dose: 120 mg/L H_2O_2 dose = 0.1 mLL^{-1}; reaction time: 2 h]; (b) Reusability tests for Fe^0-Ag^0@BN nanocatalyst in the degradation of AY under the photo-Fenton-like process

Fig. 9 (a) Degradation of AY and leaching of iron(II) vs. reaction time [pH = 3.0, nanocatalyst dosage = 120 mg/L, H_2O_2 dosage = 0.1 mL/L, reaction time = 120 min] in a dark environment; Photo-mediated Fenton-like treatment of AY in the natural water sample photo-assisted Fenton-like treatment of AY in the natural water samples (b) W1 and (c) W2 [pH = 3.0, AY = 2.0 mg/L, nanocatalyst dosage = 120 mg/L H_2O_2 dosage = 0.1 mL/L reaction time = 120 min]

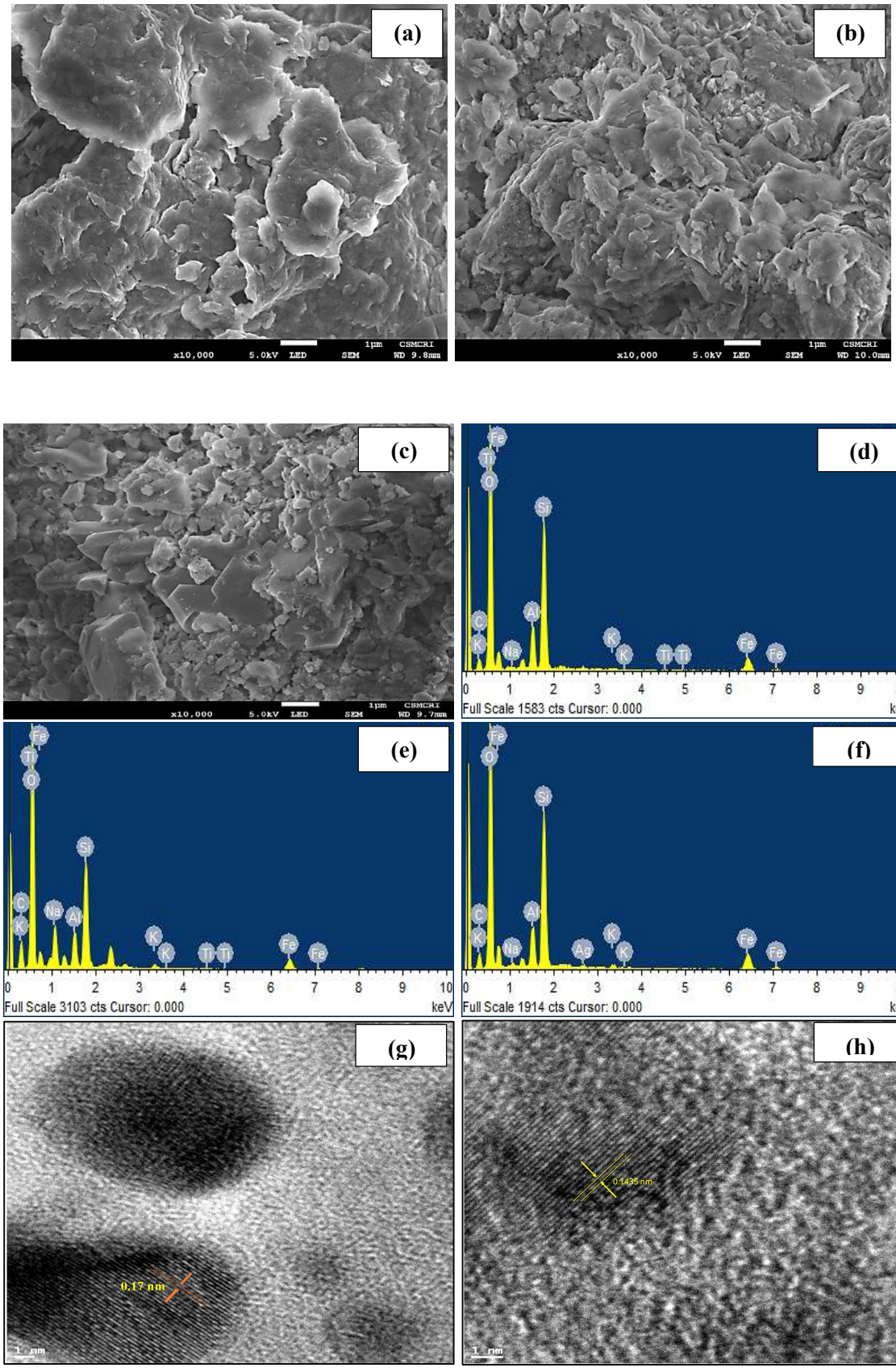

(a)
x10,000 5.0kV LED SEM WD 9.8mm
(b)
x10,000 5.0kV LED SEM WD 10.0mm
(c)
x10,000 5.0kV LED SEM WD 9.7mm
(d)
Full Scale 1583 cts Cursor: 0.000 keV
(e)
Full Scale 3103 cts Cursor: 0.000 keV
(f)
Full Scale 1914 cts Cursor: 0.000 keV
(g)
0.17 nm
(h)
0.1435 nm

Fig. 1 The SEM images of (a) BN, (b) Fe^0@BN, and (c) Fe^0-Ag^0@BN solids, the EDX spectroscopic representation of (d) BN, (e) Fe^0@BN, and (f) Fe^0-Ag^0@BN, the TEM images of (g) Fe^0@BN, and (h) Fe^0-Ag^0@BN nanocomposite solids

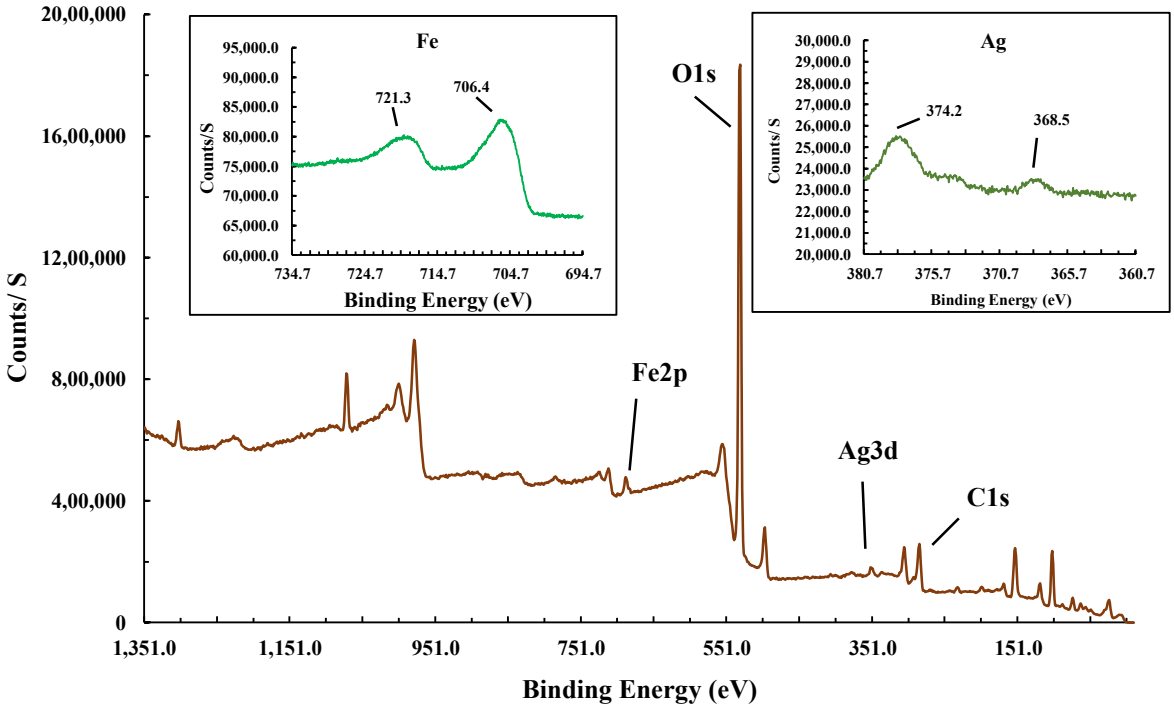


Fig. 3 The XPS spectroscopic analysis for the Fe0-Ag0@BN solids [XPS pattern of Fe and Ag in the Fe0-Ag0@BN nanocatayst]

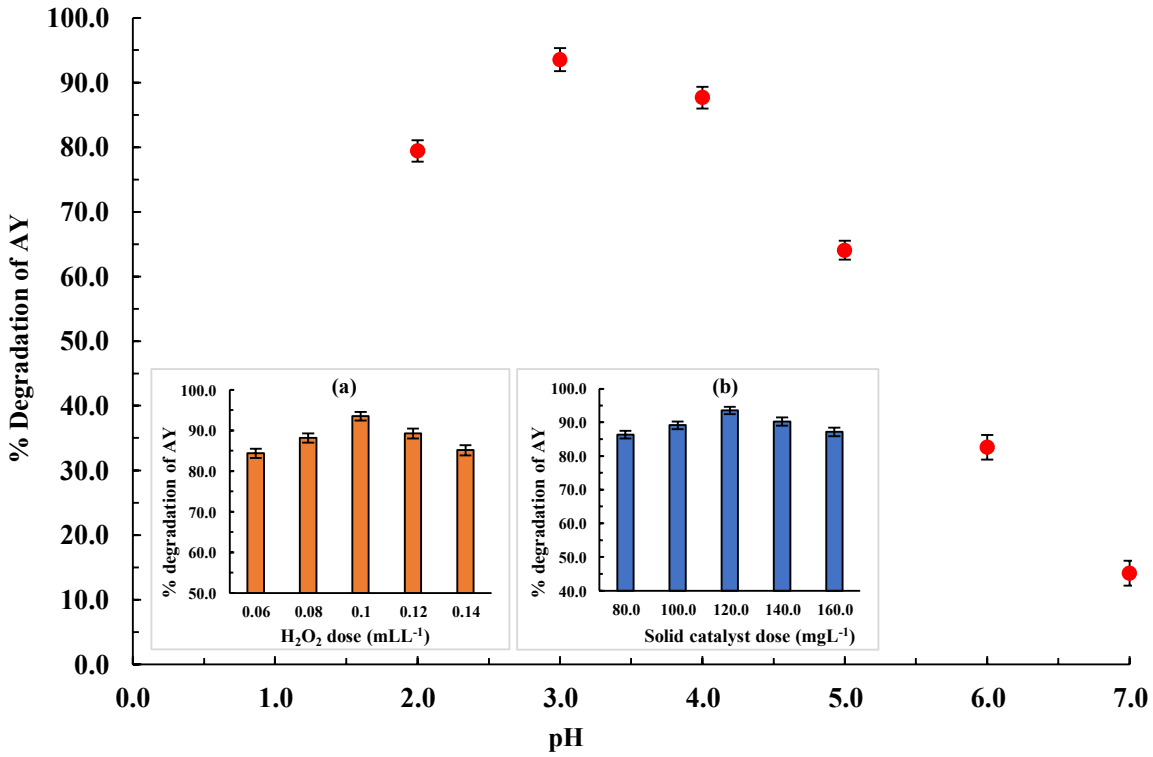


Fig. 4 Degradation percentage (%) of AY at different initial solution pH values [nanocatalyst dosage = 120 mg/L, H_2O_2 dosage (30 %) = 0.1 mL/L, AY = 2.0 mg/L, duration time = 2 h] under dark conditions [(a) Degradation of AY in the different dosages (0.06 to 0.14 mL/L) of H_2O_2 in the dark environment and (b) Degradation of AY at various dosages of Fe0-Ag0@BN in the dark environment]

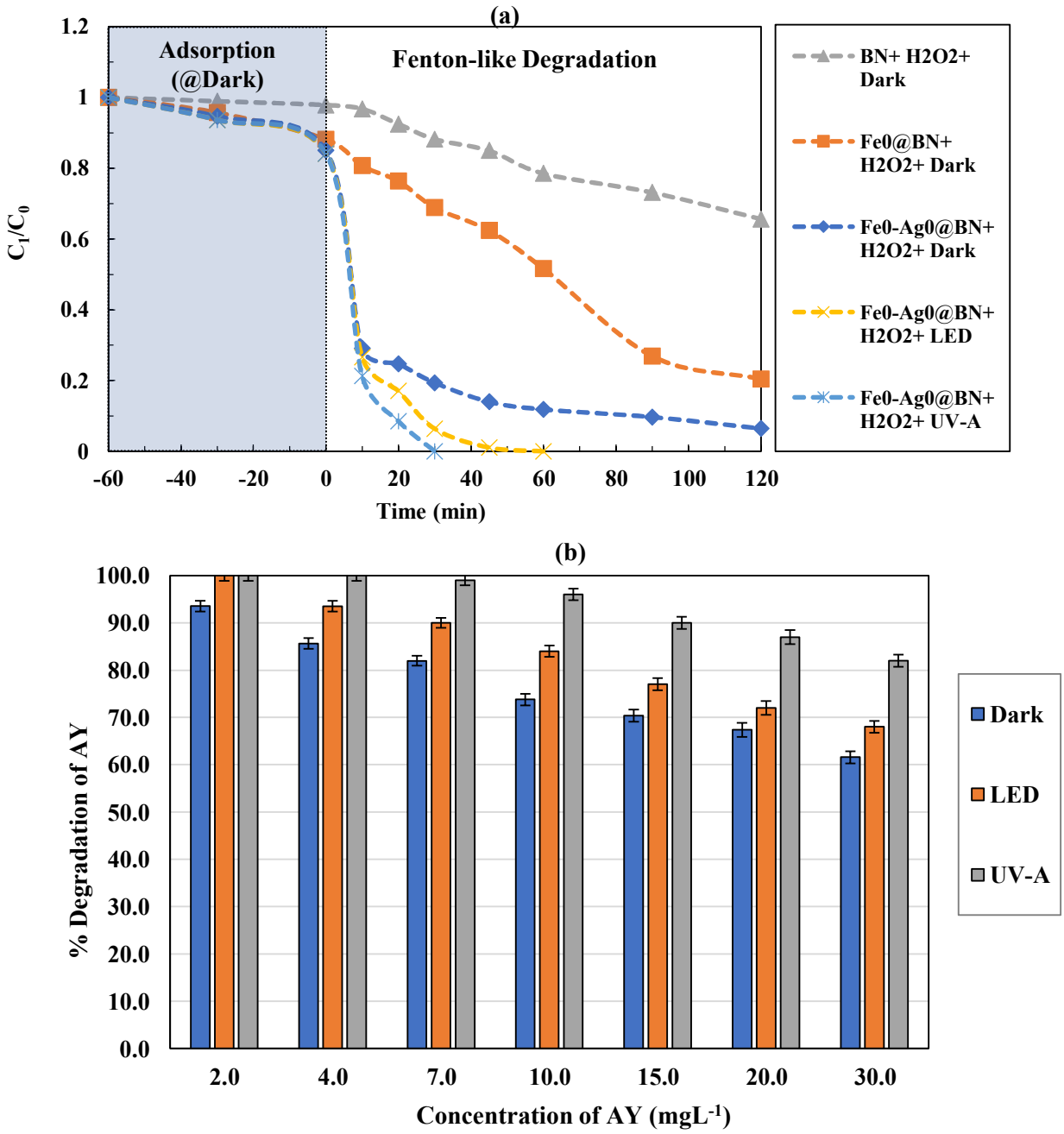


Fig. 5 (a) Degradation of AY vs. reaction time (min) in different reaction conditions [pH = 3, AY = 2 mg/L, nanocatalyst dosage = 120 mg/L, H_2O_2 dosage = 0.1 mL/L, reaction time = 120 min], (b) Influence of initial pollutant's concentration on the AY degradation under different illuminations [pH = 3, nanocatalyst dosage = 120 mg/L, H_2O_2 dosage = 0.1 mL/L, reaction time = 120 min]

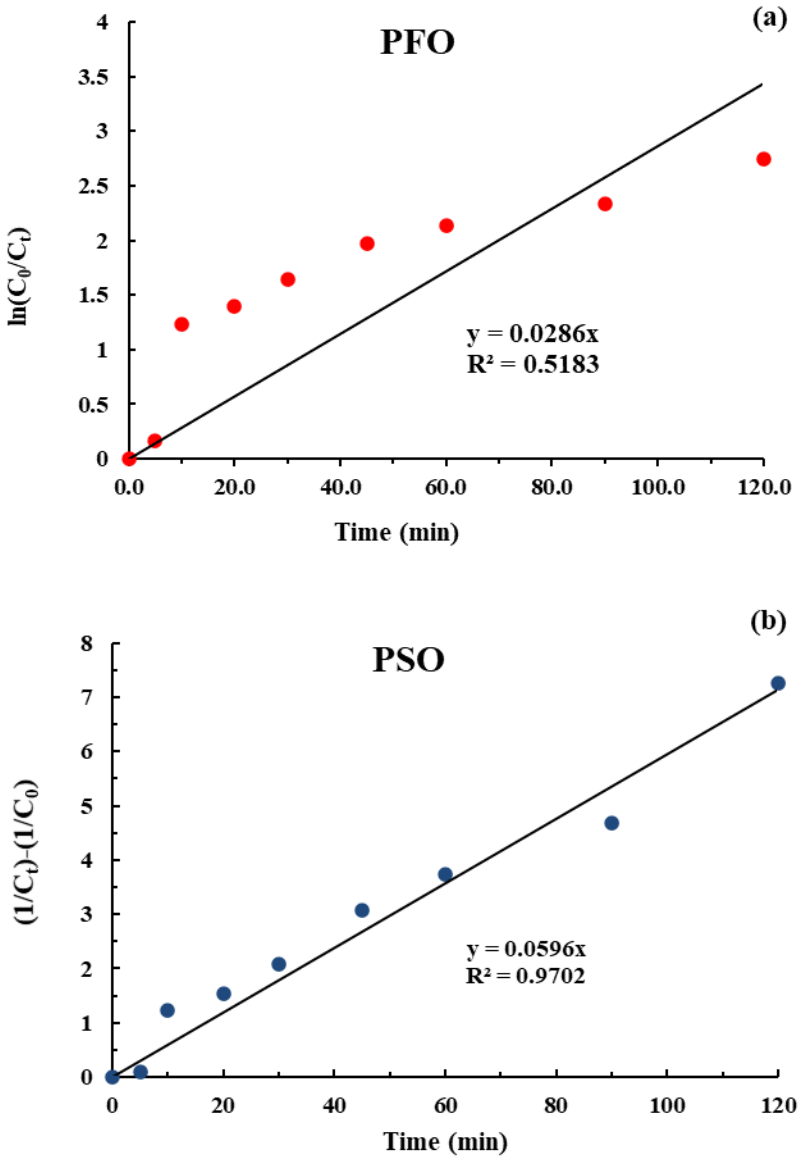


Fig. 6 The kinetics models of AY degradation, using (a) the PFO; and (b) PSO

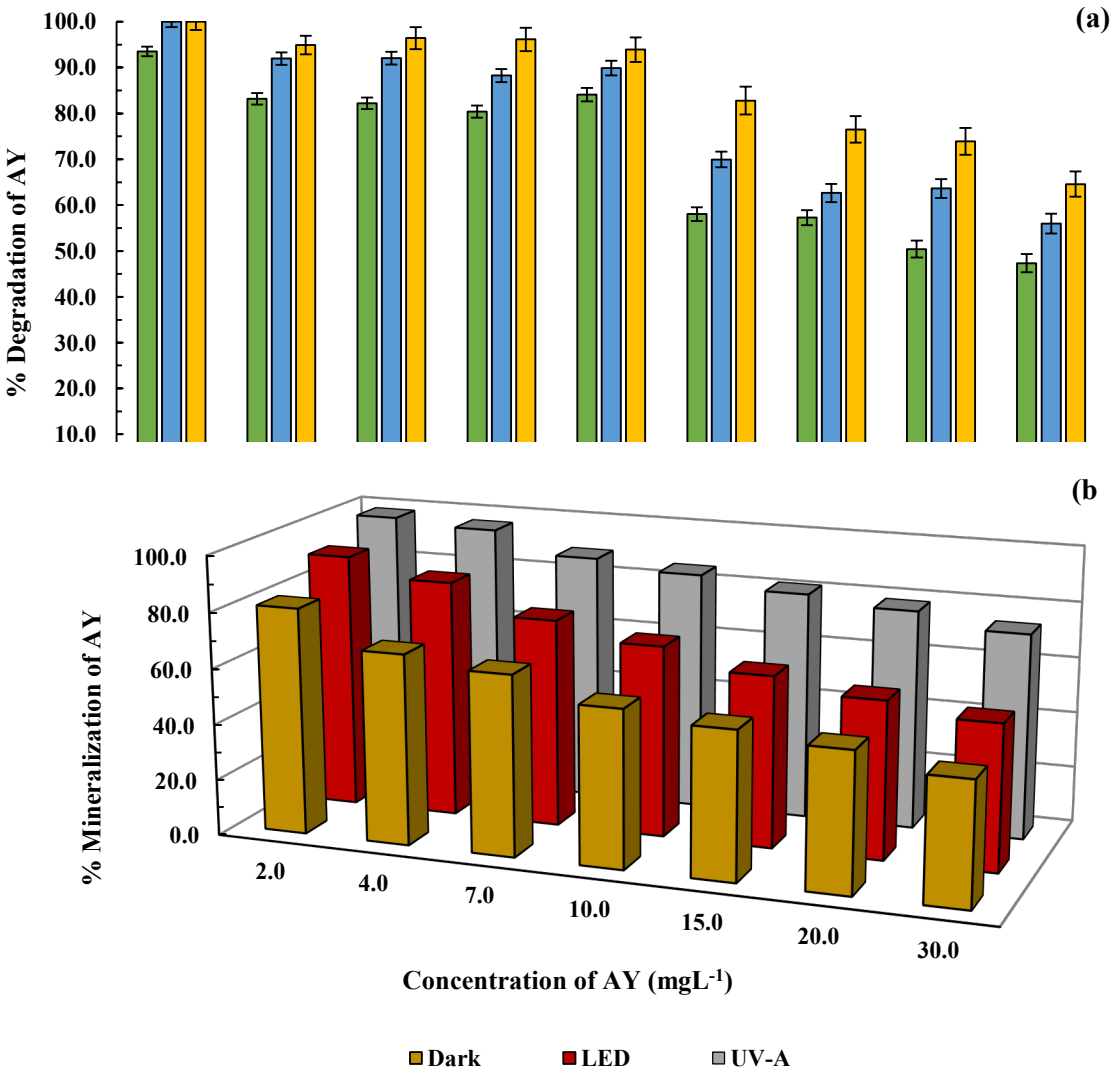


Fig. 7 (a) Impact of co-existing cations and anions in the photo-assisted Fenton-like degradation of Alizarin Yellow [pH = 3, AY = 2 mg/L, co-ions = 10 mg/L nanocatalyst dosage = 120 mg/L H_2O_2 dosage = 0.1 mL/L reaction duration = 120 min];, (b) Degradation (%) of AY at different concentrations [pH = 3, nanocatalyst dosage = 120 mg/L, H_2O_2 dosage = 0.1 mL/L, reaction duration = 120 min]

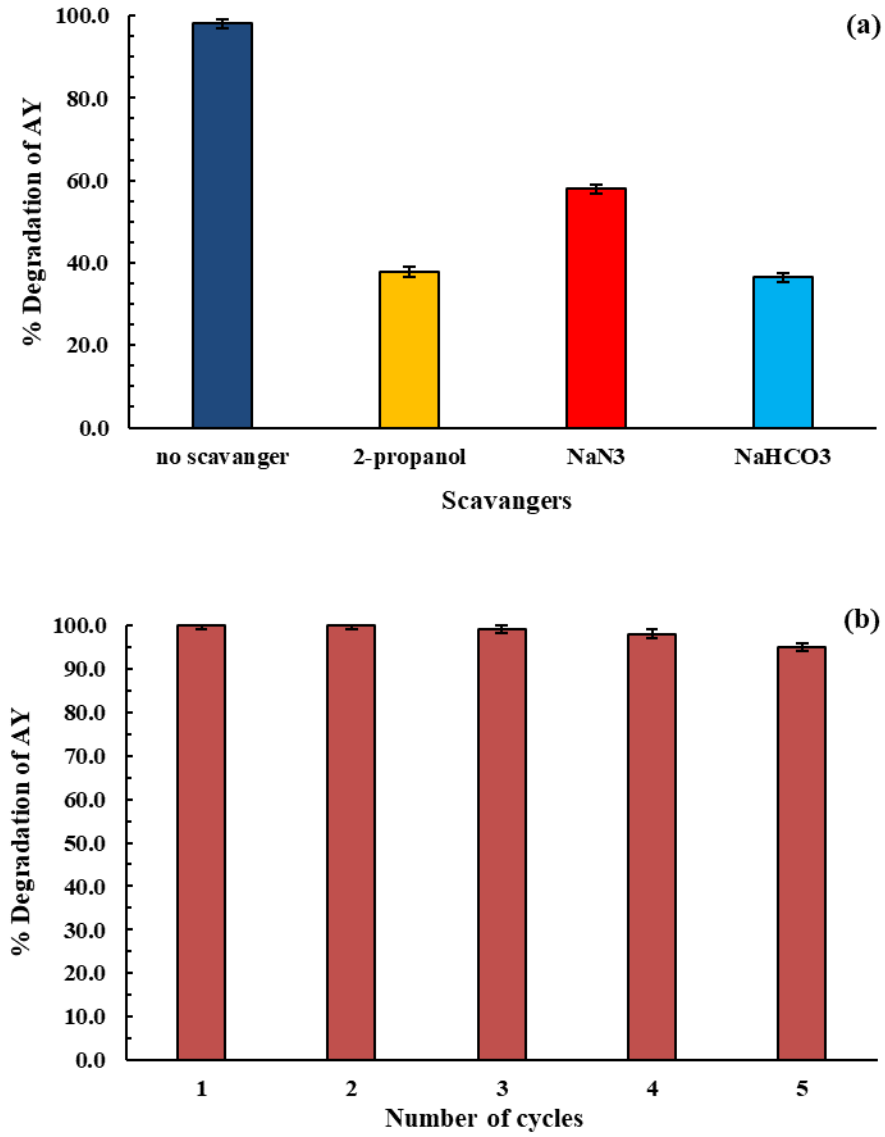


Fig. 8 (a) Impact in degradation (%) of AY in the presence of scavengers [pH = 3; AY = 2 mg/L; [scavenger]: 0.1 mol/L (1.0 mL/L); catalyst dose: 120 mg/L H_2O_2 dose = 0.1 mL/L, reaction time: 2 h]; (b) Reusability tests for Fe^0-Ag^0@BN nanocatalyst in the degradation of AY under the photo-Fenton-like process

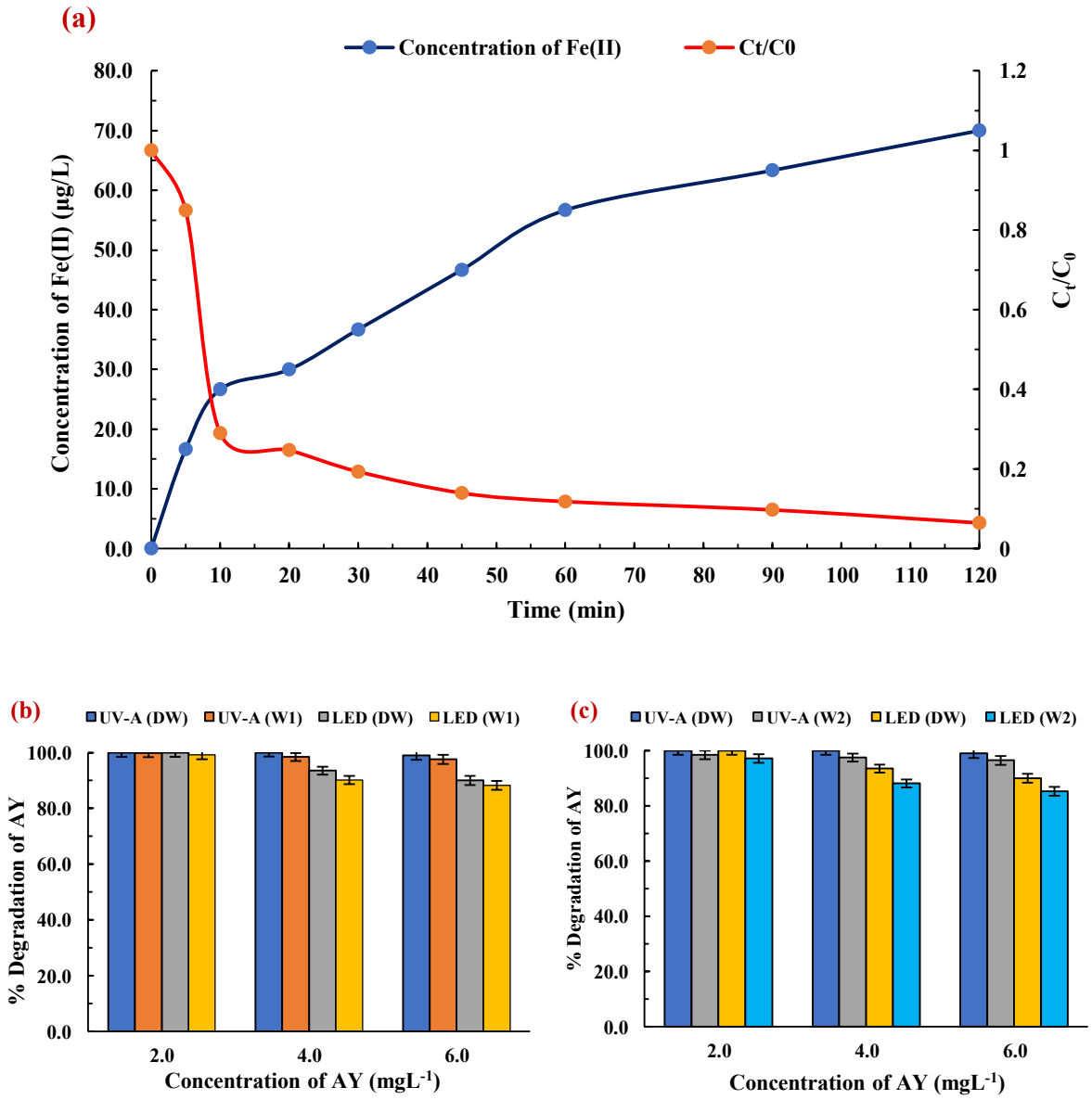


Fig. 9 (a) Degradation of AY and leaching of iron(II) vs. reaction time [pH = 3, nanocatalyst dosage = 120 mg/L, H_2O_2 dosage = 0.1 mL/L, reaction time = 120 min] in a dark environment; Photo-mediated Fenton-like treatment of AY in the natural water sample photo-assisted Fenton-like treatment of AY in the natural water samples (b) W1 and (c) W2 [pH = 3, AY = 2.0 mg/L, nanocatalyst dosage = 120 mg/L H_2O_2 dosage = 0.1 mL/L reaction time = 120 min]